Nanoscale

Accepted Manuscript

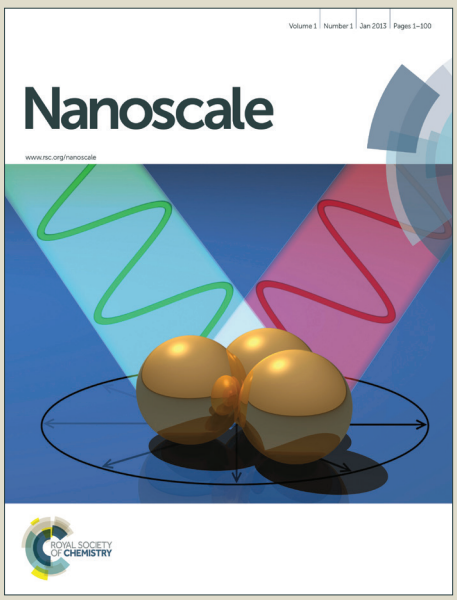

ROYAL SOCIETY OF CHEMISTRY

www.rsc.org/nanoscale

Sub-Nanometer Expansions of Redox Responsive Polymer Films Monitored by Imaging Ellipsometry

Aysegul Cumurcu, Xueling Feng, Lionel Dos Ramos, Mark A. Hempenius, Peter Schön, G. Julius Vancso*

Department of Materials Science and Technology of Polymers, University of Twente, MESA+ Institute for Nanotechnology, P.O. Box 217, 7500 AE Enschede, The Netherlands.

Abstract:

We describe a novel approach to quantitatively visualize sub nm height changes occurring in thin films of redox active polymers upon reversible electrochemical oxidation/reduction in-situ and in real-time with electrochemical imaging ellipsometry (EC-IE). Our approach is based on the utilization of a micro patterned substrate containing circular patterns of passive (non-redox active) 11-mercapto-1-undecanol (MCU) within a redox-responsive oligoethylene sulfide end-functionalized poly(ferrocenyldimethylsilane) (ES-PFS) film on a gold substrate. The non-redox responsive MCU layer was used as a molecular reference layer for the direct visualization of the minute thickness variations of the ES-PFS film. The ellipsometric microscopy images were recorded in aqueous electrolyte solutions at potentials of -0.1 V and 0.6 V vs. Ag/AgCl corresponding to the reduced and oxidized redox states of ES-PFS, respectively. The ellipsometric contrast images showed a 37 (± 2) % intensity increase in the ES-PFS layer upon oxidation. The thickness of the ES-PFS layer reversibly changed between 4.0 (± 0.1) nm and 3.4 (± 0.1) nm upon oxidation and reduction, respectively, as determined by IE. Additionally, electrochemical atomic force microscopy (ECAFM) was used to verify the redox controlled thickness variations. The proposed method opens novel avenues to optically visualize minute and rapid height changes occurring e.g. in redox active (and other stimulus responsive) polymer films in a fast and non-invasive manner.

Keywords: Imaging ellipsometry, redox stimulus, responsive film, thickness variation

1. Introduction

Growing demand for organic thin films in functional coatings, lithography resists, and other areas in nanotechnology make it inevitable to study dynamic processes such as film swelling and growth, or molecular adsorption in real time at the nanoscale.[1-9] For instance, in situ ellipsometry has been used to determine polymerization kinetics and polymer growth as well as morphological changes of polymer films upon environmental changes such as variations in solvent, temperature and pH, in real time.[1-8] The thickness changes upon oxidation and reduction for redox-active monolayers were also determined by in situ ellipsometry.[10,11] However, conventional ellipsometry lacks the possibility of direct optical visualization of morphology variations of thin films.

Imaging ellipsometry (IE), a "hybrid" of ellipsometry and optical microscopy, combines the sub-nm vertical resolution of ellipsometry with imaging capabilities of optical microscopy.[12] The morphological structures of surfaces in IE are imaged by using an objective and a CCD detector.[12,13] IE is based on the use of combined null and off-null ellipsometry. This means that while the optical signal on one area of the sample surface is minimized by null-ellipsometry conditions (areas appearing dark in the image), the off-nulled areas, simultaneously, provide a stronger signal (which appear bright in the image).[12] IE is a label free, noncontact technique with in situ measurement possibilities, therefore it is well-suited to monitor real time changes at surfaces of thin films.[14-20] For instance, using in situ IE, Schmaljohann et al. investigated the thermoresponsive aggregation behavior of a micropatterned hydrogel film in the temperature region between 35-37 ˚C.[16] The temperature dependent swelling and collapse of the hydrogel film in water was monitored by recording the ellipsometric angle, Δ. In another study by Faiss et al., the thickness variations of microstructured lipid bilayers upon temperature change were monitored by IE.[17] Ellipsometric thickness maps of 1,2-dimyristoyl-*sn*-glycero-3-phosphocholine (DMPC) bilayers showed a reversible thickness change between 13 and 46 ˚C.

IE was also combined with other techniques such as electrochemical methods and microbeam grazing incidence small angle X-ray scattering (μGISAXS).[15,18-20] For instance, in a study by Svoboda et al., in situ IE was used together with cyclic voltammetric deposition to monitor the film growth of conductive biocatalytically polymerized methylene green (poly-MG) films on platinum surfaces.[15] It was shown that the film growth was homogenous and resulted in

an evenly distributed polymer layer. Another hybrid IE technique was introduced by Körstgens et al.[18] In their study μGISAXS was coupled to an IE for structural and morphological characterization of nanostructures. To illustrate the capabilities of this tool, kinetics of the self-assembly of colloidal polymer nanospheres on a rough substrate were studied.[18] In another study by Yu et al., IE was combined with electrochemical methods to study electrostatically driven adsorption of proteins at solid surfaces in real time.[19] We finally mention, that Liu et al. used total internal reflection imaging ellipsometry (TIRIE) to monitor protein interaction processes in real time.[20]

Macromolecules which contain organometallic groups or inorganic elements in their main chain are of particular interest in current research, since they not only possess the processability of polymers but also possess highly interesting optical, electrical, magnetic and chemical characteristics related to the inorganic (or organometallic0 groups.[21-23] Poly(ferrocenylsilanes) (PFSs), containing alternating ferrocene and silicon units in their main chain, belong to this group of materials.[24,25] PFS is a redox active polymer which can be partially or fully oxidized using chemical or electrochemical procedures.[26-29] Therefore, PFS found use in various application areas including ion recognition, biosensors, electrochemical sensing and molecular release.[30-32] Additionally, PFS was used as resist in different lithography techniques, such as UV photolithography, electron-beam (e-beam) lithography, block copolymer lithography, as well as in more traditional lithography processes as an etch mask. The resulting metal-rich masking nano-structures offer etch resistance, catalytic, optical, sensing, electrical and magnetic properties.[33-36]

The electrochemically induced morphology and volume changes of surface grafted PFS layers and also other redox-active polymers, such as polypyrrole (PPy) and polyaniline (PANI), were previously studied by spectroscopic ellipsometry and surface plasmon resonance spectroscopy under electrochemical control.[10,37,38] Electrochemical atomic force microscopy (EC-AFM) and microscopic observation simultaneously with voltammetric experiments were imaging techniques used to visualize the associated morphology changes.[10,37-40]

Soft lithography techniques including microcontact printing (μCP), replica molding (REM), microtransfer molding (μTM), micromolding in capillaries (MIMIC), solvent assisted micromolding (SAMIM) etc. are cost-effective and fast microfabrication methods.[41-45] Soft lithography techniques allow one to control the chemistry of the patterned surfaces and to manufacture patterned surfaces with complex organic groups found in biology and biochemistry.[46] Patterned elastomers, such as polyurethanes, polyimides, poly(dimethylsiloxanes) (PDMS), are used as stamps in all soft lithography techniques.[47] We shall use μCP in this study to obtain patterned surfaces allowing for accurately measuring thickness variations in the sub-nm range.

In this work the redox-induced morphology and volume changes of an oligoethylene sulfide end-functionalized poly(ferrocenyldimethylsilane) (ES-PFS) film on a gold substrate was visualized versus a 11-mercapto-1-undecanol (MCU) layer in situ by electrochemical imaging ellipsometry (EC-IE). A micro-patterned film of the MCU layer (100 μm diameter circles) was prepared by μCP and subsequently the unpatterned areas were filled with the ES-PFS layer. The MCU film served as zero-level, inert reference layer to monitor sub nm thickness variations of the ES-PFS film. The thickness changes were verified in situ by IE and AFM under electrochemical control. This strategy allows one to precisely and accurately measure thickness changes, and simultaneously observe at film surfaces morphology variations. This approach may find applications in studies of thin film erosion, photoresist pattern development, use of responsive layers in (bio)sensing and actuation, in fluidics, and other nanotechnologically relevant areas.

2. Experimental Section

2.1. Materials

MCU and 1H,2H,2H-perfluorodecyltrichlorosilane were purchased from Sigma-Aldrich. PDMS prepolymer (Sylgard silicone elastomer 184) and curing agent (Sylgard silicone elastomer 184 curing agent) were acquired from Dow Corning Corporation. Tetrahydrofuran (THF) and ethanol were provided by Biosolve (Valkenswaard, The Netherlands). Hydrogen peroxide (H_2O_2) 30% was obtained from Merck (Darmstadt, Germany). Sulfuric acid (H_2SO_4) 95-97% was obtained from Sigma-Aldrich (St. Louis, MO, USA). All materials were used as received. Milli-Q water was produced by a Millipore Synergy system (Billereca, MA, USA). ES-PFS (M_n=

22500 g/mol, M_w/M_n=1.16) was prepared by treating living PFS with ethylene sulfide according to a previously published procedure.[29]

2.2. Sample Preparation

Gold substrates (silicon wafer, 10 nm chromium adhesive layer and 100 nm gold layer, dimensions: 2.5×1.5 cm^2) were prepared using a Balzers BAK 600 evaporation system. Prior to use, the gold substrates were cleaned in piranha (30% H_2O_2/70% H_2SO_4) for 20 s and rinsed with Milli-Q water and ethanol. Subsequently the substrates were dried in a stream of nitrogen. *Caution! Piranha solution is a very strong oxidant and reacts violently with organic materials and should be handled with utmost care!* The elastomeric stamp was prepared by pouring a mixture of PDMS prepolymer and its curing agent (10:1 by weight) onto a silicon master with featured a hole array of 100 μm circles at a depth of 600 nm. Prior to use, the master was treated with an anti-adhesion layer of 1H,1H,2H,2H-Perfluorodecyltrichlorosilane to facilitate remolding. The master had dimensions of 1.5×1.5 cm^2 with a patterned region of 1×1 cm^2. After curing at 70℃ for 12 hours, the PDMS was carefully peeled off the stamp at room temperature. The feature of the master was transferred to the PDMS stamp as pillars of the same dimensions.

A 2 mM solution of MCU in ethanol was used as ink for the μC printing. First the ink solution was applied to the surface of the PDMS stamp by a cotton Q-tip and then dried with a stream of N_2 for ~1 min.[48,49] The dry PDMS stamp not having ink visible on the surface, was brought into contact with the gold substrate for 30 s. It is important to note that gentle tapping on the PDMS stamp may be needed to ensure that air bubbles are not trapped between the PDMS stamp and the gold substrate.[50] After removing the stamp, a 5 mL solution of ES-PFS (1 mg mL^{-1} solution in THF) was poured on the substrate. Next, the substrate was washed with large amounts of THF and ethanol at room temperature. Finally, the substrate was dried in a stream of nitrogen.

2.3. Characterization Techniques

2.3.1. Electrochemical Imaging Ellipsometry

In-situ IE measurements were performed with a Multiskop imaging ellipsometer (Optrel, Kleinmachnow, Germany) under electrochemical potential control with an Autolab PGSTAT10 potentiostat (Ecochemie, Utrecht, The Netherlands) in a liquid cell with a volume of 0.7 mL and PEEK cover and Teflon tubing (Nanofilm surface analysis, Halcyonics GmbH). The angle of

incidence was set to 60˚, which assured that the light path was oriented normal to the window of the liquid cell.[16] The IE was operated in the Polarizer-Compensator-Sample-Analyzer (PCSA) configuration. The local height profile of the polymer film was obtained using a microscope objective (M-Plan APO 10×, Mitutoyo, Neuss, Germany) and a CCD camera with a resolution of 640×480 pixels. The sample was illuminated with a He-Ne laser ($\lambda = 632.8$ nm). The electrochemical experiments (cyclic voltammetry) were performed in a liquid cell with a three-electrode configuration. The gold substrate with the polymer coating was used as working electrode, in combination with Ag/AgCl reference and Pt counter electrodes, respectively. The measurements were performed in 0.1 M $NaClO_4$ aqueous solution. The cyclic voltammograms were recorded between -0.1 and 0.6 V (versus Ag/AgCl) at 50 mV s^{-1} scan rate. The IE images were captured after keeping the sample at potentials of -0.1 and 0.6 V for two minutes each, to insure the complete redox response of the whole polymer layer. The images were corrected for the distortion caused by the oblique angle of incidence.[12] Thicknesses of the ES-PFS layers were determined by IE from the selected region of interests (ROIs) containing the ES-PFS layers on the sample surface. A commercial software supplied with the Multiskop setup was used to fit a three–layer model (gold/ES-PFS/water) using Fresnel's theory.[51] The refractive index of the ES-PFS layer was taken as n=1.687 for both the oxidized and the reduced states, respectively.[10] Refractive index and the extinction coefficient of the gold substrate were determined experimentally by ellipsometry as 0.175 and 3.519, respectively.

2.3.2. Electrochemical Atomic Force Microscopy

AFM measurements were performed in a combined electrochemical AFM (EC-AFM) setup using a Multimode 8 AFM (Bruker Nano Surfaces, Santa Barbara, CA, USA) with a NanoScope V controller and an electrochemical liquid cell in combination with an Autolab PGSTAT10 potentiostat (Ecochemie, Utrecht, The Netherlands). Commercially available V-shaped silicon nitride cantilevers (DNP, Bruker AFM probes, Camarillo, CA, USA) with nominal spring constants of 0.35 N/m were used for imaging. Peak Force Tapping Mode AFM was done at a constant oscillation of the sample at 2 kHz using amplitudes of 30-120 nm and peak forces of 100 pN. Scanning was performed at a rate of 0.977 Hz. The ECAFM experiments were carried out in a closed electrochemical liquid cell (DI) with approximately 50 µL inner volume. The liquid cell contained a three-electrode system including the polymer covered gold substrate as working, a Pt

wire as counter and Ag as reference electrode. A 0.1 M $NaClO_4$ aqueous solution was used as electrolyte. The potential was cycled between -0.2 and 0.6 V at a scan rate of 50 mV s^{-1} and the AFM height images were captured after keeping the sample two minutes at the oxidized or reduced state, respectively. Before and after AFM imaging, cyclic voltammograms were recorded to determine the surface concentration of the PFS and to verify proper electrochemistry of the modified substrate. Image processing and data analysis were performed with the NanoScope software, version 8.15, and NanoScope Analysis software, version 1.4. To quantify the average height variation, step analysis was performed which makes relative height measurements between two regions (steps) on sample surfaces.

It should be noted that the EC-IE and EC-AFM measurements were done with different set-ups and electrochemical liquid cells. While for the EC-AFM measurements a silver wire was used as reference electrode, for the EC-IE measurements an Ag/AgCl electrode was used. Therefore, the respective minimum and maximum vertex potentials were chosen according to the specific cyclic voltammogram recorded for each experiment, proofing complete oxidation or reduction, respectively. Accordingly, a slightly more positive potential was chosen for the EC-AFM (-0.1V) compared to the EC-IE experiments (-0.2V).

3. Results and Discussion

In this study, the redox-induced morphology and volume changes of a ES-PFS film on gold were monitored in situ by EC-IE. For this purpose, a micro-patterned ES-PFS/MCU sample was prepared on a gold substrate by μCP. The sample preparation steps are shown in Fig. 1. Firstly, the MCU layer was printed on a gold substrate using a PDMS stamp (Fig. 1, step 1 to 4). Next, the un-patterned areas on the gold substrate were filled with the ES-PFS layer by pouring the ES-PFS solution on the sample (Fig. 1, step 5). Subsequently, the sample was washed with large amounts of THF and ethanol to remove any traces of physisorbed ES-PFS and MCU layers (Fig. 1, step 6). Finally, the as-obtained ES-PFS/MCU sample contained circular patterns of non-redox active MCU with a surrounding redox active ES-PFS layer (Fig. 1, step 7).

As we expect sub-nanometer thickness variations in ES-PFS films, it is important to define an inert zero level as reference. Thus it is of pivotal importance to exclude possible nonspecific adsorption of PFS to the MCU patterns. In order to determine the adsorption of ES-PFS on the

MCU layer, a non-patterned sample was prepared first by immersing the gold substrate into the MCU solution overnight to form the thiol monolayer on the entire gold surface. The same amount of ES-PFS solution was poured on this sample as in the micro-patterned ES-PFS/MCU sample preparation and the sample was then washed with the same amount of THF and ethanol. The XPS spectra of this non-patterned sample did not show any traces of Fe, proving the absence of ES-PFS on the MCU pattern after this fabrication procedure. The information is provided in the supplementary material (Fig. S1).

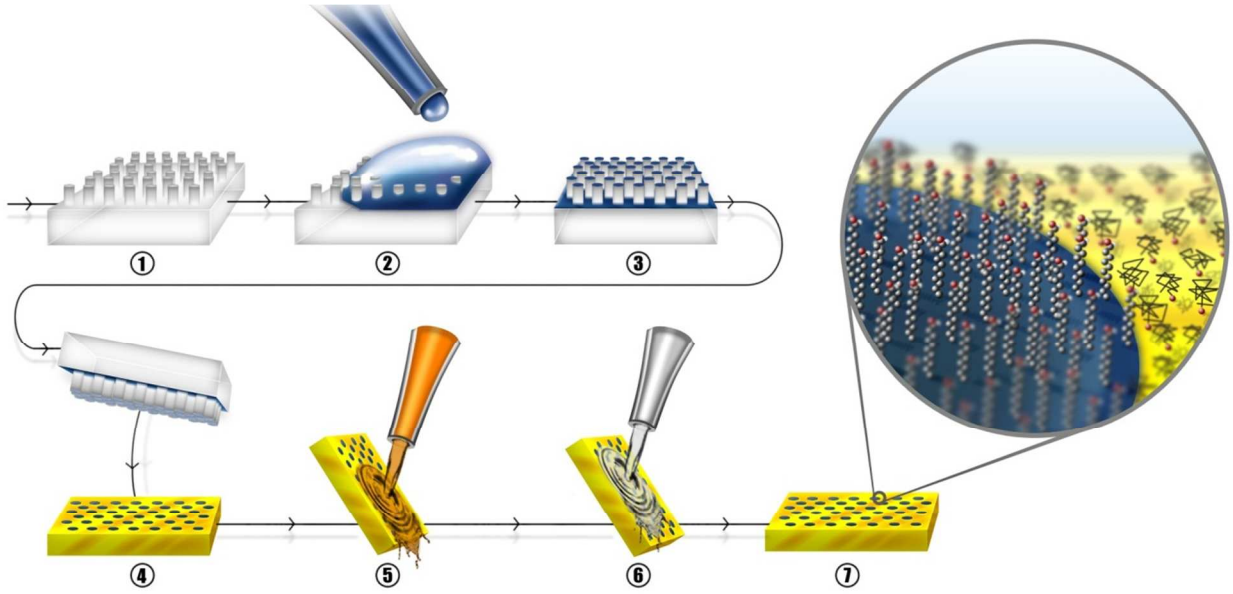

Fig. 1. Preparation of the micro-patterned ES-PFS/MCU sample by μCP: (1) PDMS elastomeric stamp with pillars, (2) the stamp was covered by the ink solution of MCU, (3) the stamp was dried until no visible ink remains, (4) the ink was printed by contacting the inked stamp with a gold substrate, (5) ES-PFS solution was poured onto the MCU patterned gold substrate, (6) the substrate was washed with THF and ethanol, (7) the final micro-patterned ES-PFS/MCU sample. The inset in the step 7 shows a zoomed scheme of the patterned MCU monolayer (represented with a blue background) and the ES-PFS layer present on the outside of the patterned area (represented with a yellow background).

A cyclic voltammogram (CV) of the micro-patterned ES-PFS/MCU sample on a gold substrate, recorded with the EC-IE, is shown in Fig. 2. The double-wave peaks in the CV are indicative for PFS and reflect the intermetallic coupling between neighboring iron centers in the polymer chain.[10,27,29] In the first oxidation wave, ferrocene units in alternating positions are

oxidized, generating positively charged ferrocenium (Fc^+) moieties, followed by oxidation of the remaining ferrocenes in the second wave at higher potential.[52,53] Broadening of the second oxidation wave is attributed to intermetallic interactions with a variable number of oxidized neighboring units.[10]

The surface coverage of the ferrocene sites (Γ_{Fc}) was calculated as 1.76×10^{-9} mol cm^{-2} using the following equation;

$$\Gamma_{Fc} = \frac{Q_{Fc}}{nFA}, \quad (1)$$

where n is the number of electrons involved in the electron transfer (here $n_e = 1$), F is the Faraday constant ($F = 96\,485$ C mol^{-1}), A is the geometric surface area of the electrode ($A = 1$ cm^2). Q_{Fc} is the charge passed for the oxidation/reduction of ferrocene sites and was determined by integrating the areas under the redox peaks. This corresponds to a number of grafted chains per unit area of 0.17 chains nm^{-2}. The surface coverage was calculated using a cyclic voltammogram of a full ES-PFS layer prepared on a gold substrate by the same procedure of the ES-PFS filling of the micro-patterned ES-PFS/MCU sample. The corresponding cyclic voltammogram is provided in the supplementary information (Fig. S2). This full ES-PFS layer was used to determine the surface area of the ES-PFS accurately. A previous study on ES-PFS layers reported a surface coverage of 2.3×10^{-9} mol cm^{-2} for the ES-PFS with 50 repeating units (note that here we use ES-PFS with 60 repeating units).[27] The difference in the surface coverage is due to the significantly shorter immersion time of the gold substrate in the ES-PFS solution in the present procedure. A short immersion time substantially reduces the chance of physisorption of the ES-PFS on the MCU layer.

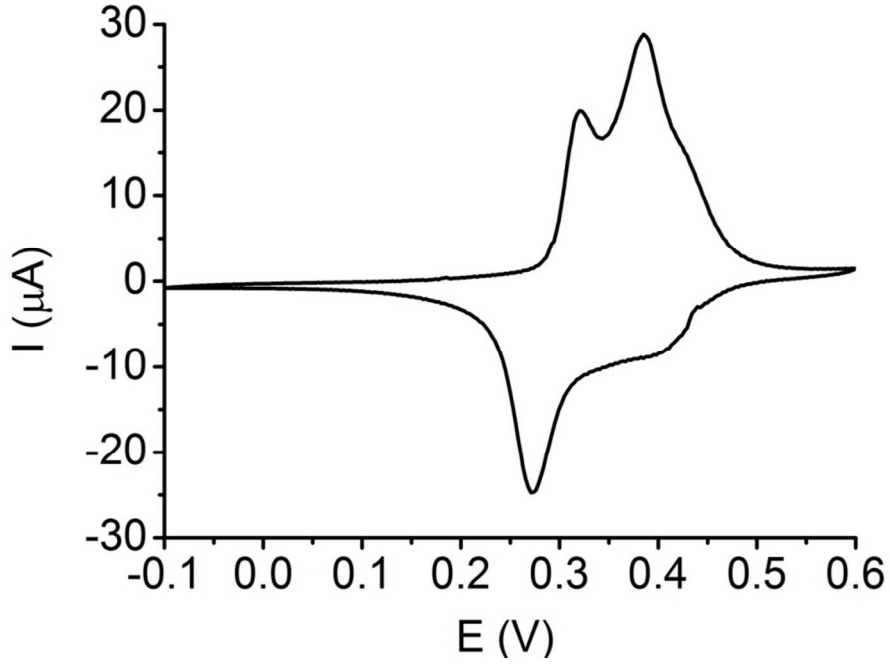

Fig. 2. Cyclic voltammogram recorded for a patterned PFS/MCU monolayer on a gold substrate at a scan rate of 50 mV s^{-1} in 0.1 M $NaClO_4$ with a Ag/AgCl reference electrode, and a Pt counter electrode.

The thickness changes induced upon electrochemical oxidation and reduction were monitored in situ by EC-IE. Fig. 3 shows the graphs of ellipsometric angles (Δ and ψ) and the film thicknesses measured at oxidized and reduced states of the ES-PFS layer, respectively. The measurements for the oxidized and reduced states were recorded after keeping the potential at 0.6 and -0.1 V for 2 min. In cycle 1 (Fig. 3), the ES-PFS layer was in the oxidized state revealing a film thickness of 4.1 nm corresponding to $\Delta = 120.814^{\circ}$ and $\psi = 44.063^{\circ}$. The film was then electrochemically reduced by keeping the potential at -0.1 V for 2 min and showed $\Delta = 121.206^{\circ}$ and $\psi = 44.147^{\circ}$ values corresponding to a film thickness of 3.4 nm (depicted as cycle 2 in Fig. 3). Repetitive cycling proved reversibility of the thickness changes upon oxidation and reduction. The average thickness increase was found to be 20% upon oxidation over three ROIs of ES-PFS. The thickness increase of the PFS layer upon oxidation was due to repulsive interactions between Fc^{+} centers in the polymer, and chain stiffening of the oxidized backbone.[10,54] In a previous study thickness changes of ES-PFS layers were determined upon oxidation via surface plasmon resonance spectroscopy (SPR) and spectroscopic ellipsometry.[10] SPR measurements, using a

He/Ne laser with a wavelength of 632.8 nm, revealed that the thickness increase from the neutral state to the fully oxidized state was 19 % for a ES-PFS layer chains with degree of polymerization DP_n=50. Spectroscopic ellipsometry measurements, performed in the visible region between 310 and 820 nm, showed that the thickness change of the same layer upon oxidation is 14 %, in very good agreement with the results presented here.[10] (We note that possible variations may be due to differences in the grafting density, in combination with chain length differences.)

As seen in Fig. 3 ellipsometric angles decrease upon oxidation and increase upon reduction. The change in Δ (~0.38˚) upon oxidation and reduction is much larger than the change in ψ (~0.07˚). This is expected since for thin films ψ is much less sensitive to thickness changes compared to Δ.[55] It is also important to note that the IE instrument standard deviations of ψ and Δ are approximately 0.004˚. This value was determined from the ES-PFS layer on a gold substrate in aqueous $NaClO_4$ solution by recording the ellipsometric angles on the same area. The standard deviations of the ellipsometric angles were calculated from 22 data points and averaged over the values determined from three different areas. Additionally, the MCU layer thickness was found to be 1.6 ± 0.2 nm. The thickness of the MCU layer did not change upon oxidation and reduction, since it did not contain any redox active units.

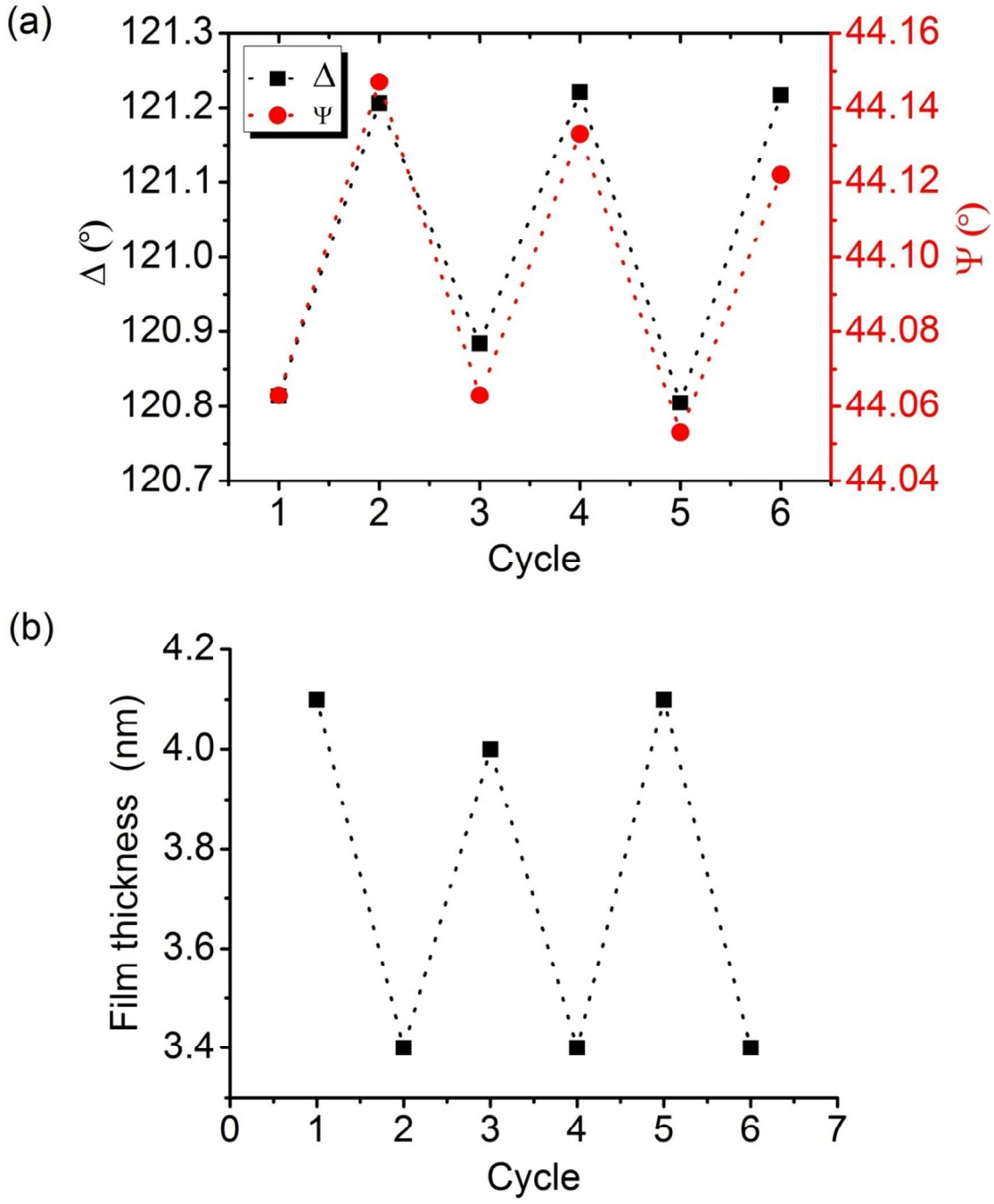

Fig. 3. Ellipsometric data and film thickness of the ES-PFS layer: In (a), Δ (left) and ψ (right) variations and in (b) the film thicknesses are plotted versus oxidation and reduction cycles. The first cycle represents the oxidized state. The dotted lines are included for guidance.

EC-IE was used to visualize the redox induced thickness change of the ES-PFS layer. Fig. 4 shows the ellipsometric contrast images of the ES-PFS/MCU sample collected in situ with EC-IE and the average intensity changes for the ES-PFS and the MCU layers. The ellipsometric contrast image represents the reflected light intensity detected by the CCD camera at the optimized position of the polarizing components to obtain maximal contrast and lateral resolution of the pattern. With the nulling mode, the signal on one area of the sample surface is minimized while the other non-nulled areas provide a strong signal simultaneously. The images in Fig. 4a and b show the real time intensity at the reduced and the oxidized states of the sample, respectively. The MCU layer (the circular areas) and the ES-PFS layer (surrounding areas) revealed different intensities due to the thickness and refractive index differences of the layers. However, more importantly, the images showed a clear intensity increase for the ES-PFS regions upon oxidation, while the MCU regions maintained the same intensity. This result was attributed to the change in the optical thickness of the ES-PFS layer upon oxidation due to conformational changes in the polymer chains by the increase in the charge density. The intensity in the central part of the ellipsometric contrast images is higher than in the margins due to the focus of the laser beam. However, the intensity change of the ES-PFS layer between the reduced and oxidized states is the same for all areas of the image.

The average intensities of the ES-PFS and MCU layers were determined over five cross-sections of 100 μm distances by averaging 450 data points in each cross-section. The intensity of the ES-PFS layer was increased by 37 ± 2% upon oxidation as compared with the zero level reference MCU layer. IE as a relative approach provides higher sensitivity since it did not require data fitting to simulations and assumptions such as the refractive index of the polymer film, the medium and the material density uniformity. Additionally, since IE is a fast, non-destructive method that can visualize large scan sizes, it is a better suited technique for determining the changes in the dynamic processes compared to other imaging techniques such as AFM, for instance.

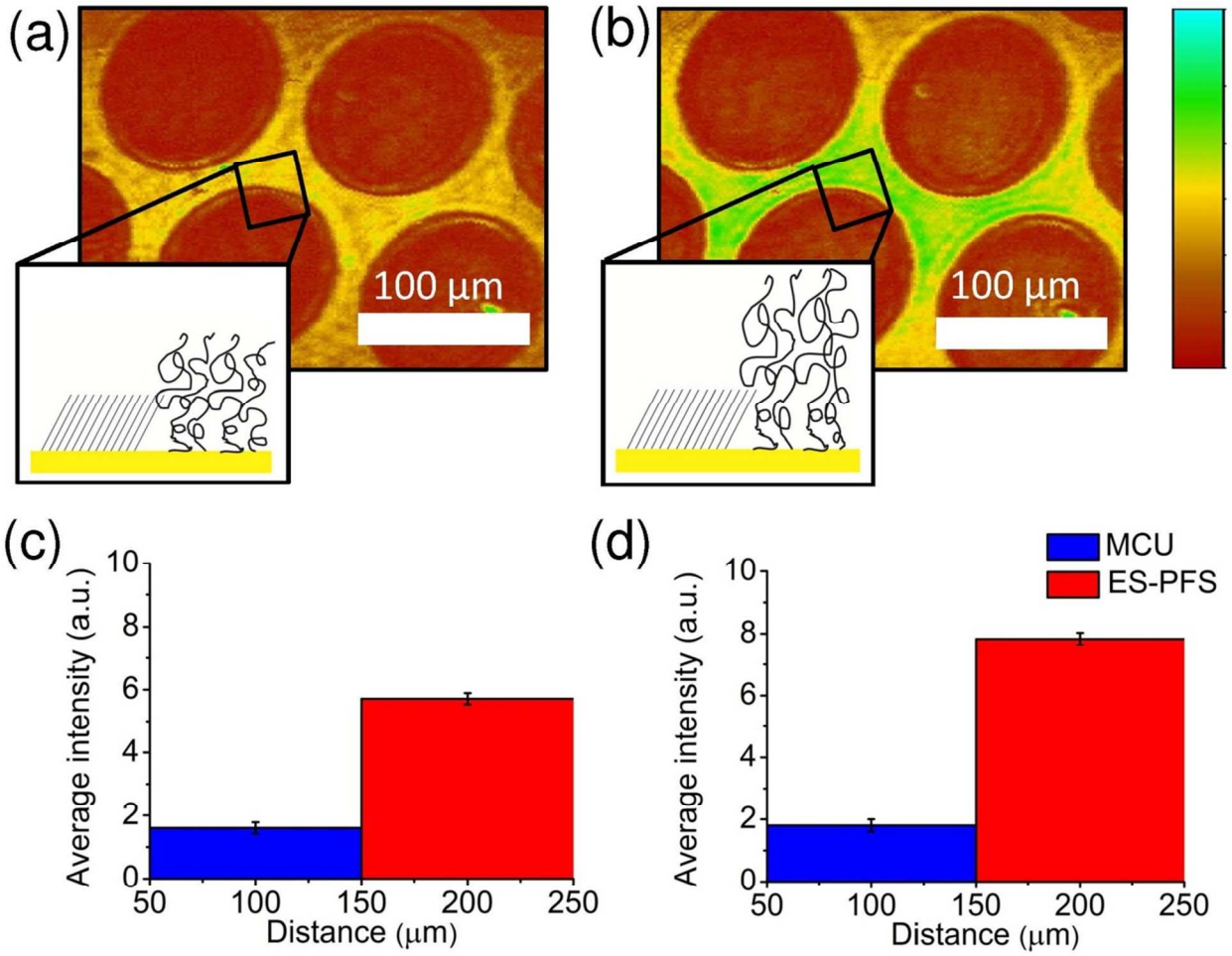

Fig. 4. Ellipsometric contrast images of the micro patterned ES-PFS/MCU sample captured at potentials of (a) -0.1 and (b) 0.6 V vs Ag/AgCl. Images were collected in situ by a combined IE-cyclic voltammetry setup. The insets in (a) and (b) show the schemes of the thickness changes of the ES-PFS layer against the stationary MCU layer. The graphs in (c) and (d) show the average intensities of the MCU (blue column) and ES-PFS (red column) layers determined from the images captured at the potentials -0.1 and 0.6 V, respectively. The average intensities were calculated from five cross-sections over a 100 µm distance with 450 data points on each cross-section for the both layers. The error bars show the standard deviation of the average intensities.

The real time ellipsometric microscopy images were also recorded with EC-IE, continuously while cycling the potential between -0.1 V and 0.6 V in a video recording. This recording is provided in the supplementary material and shows the reversibility of the thickness change simultaneously with the potential change. In addition the movie provides further evidence for the

2 step oxidation, as can be seen from a corresponding stepwise intensity increase and decrease upon reduction, respectively.

EC-AFM was used to verify the thickness changes of the ES-PFS layer against the stationary MCU layer in situ as a function of the applied potential (Fig. 5). The topography of the micro patterned ES-PFS/MCU sample was imaged at potentials -0.2 and 0.6 V. The ES-PFS layer reveals a rougher surface at the oxidized state compared to the reduced state. The height difference of the ES-PFS layer from reduced to oxidized state was 0.6 nm which corresponds to a height change of 18% against the stationary MCU layer. Here peak force tapping AFM was applied which utilizes the maximum loading force as feedback and thus operates in the repulsive contact regime. In this manner, possible influences on the measured height profiles due to variations of electrostatic interaction are essentially eliminated.

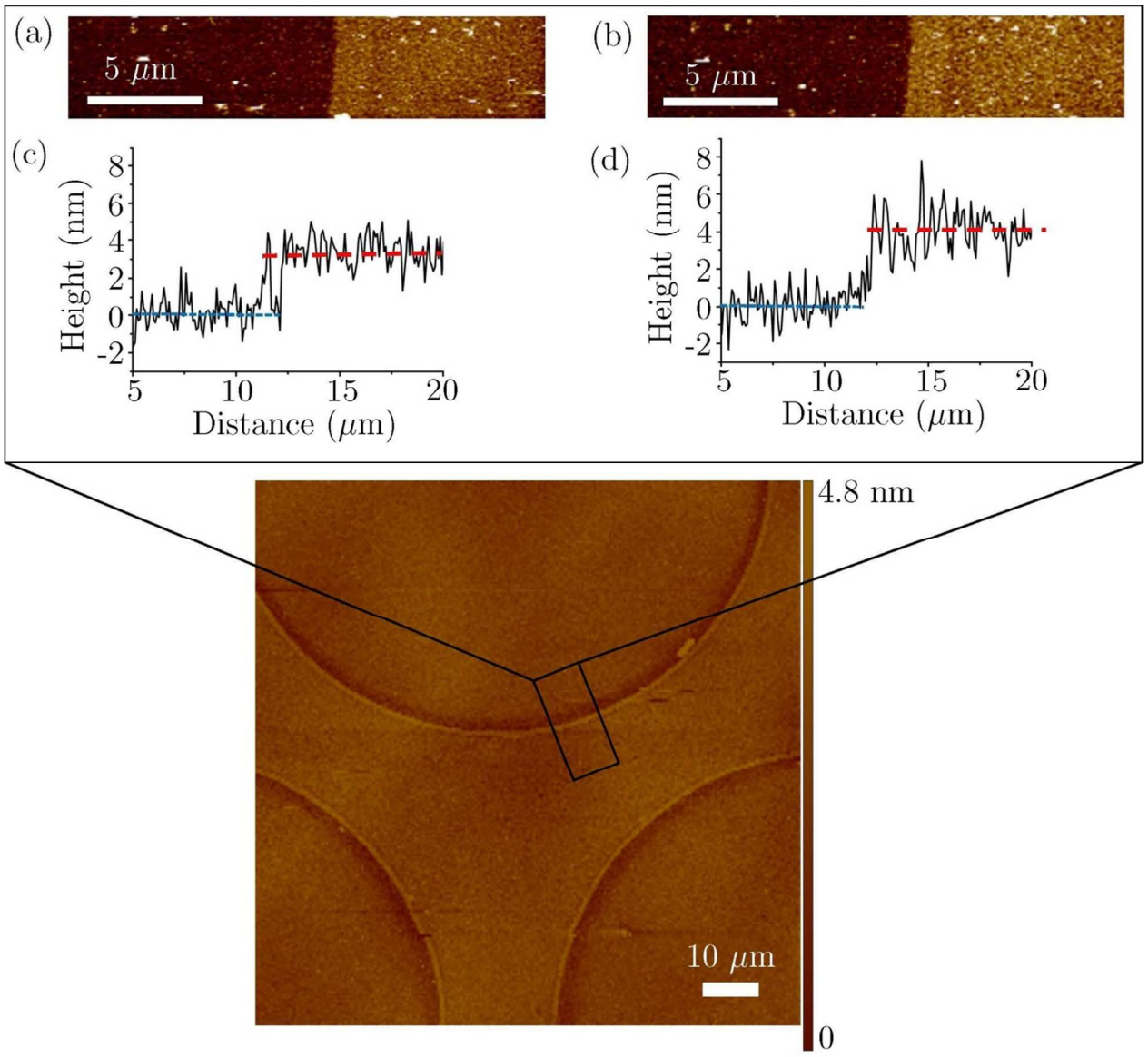

Fig. 5. EC-AFM topography images of the micro patterned ES-PFS/MCU sample: the large scale image at the bottom shows the AFM image of the micropatterned structure of the sample. The inset (top images) shows a zoomed area indicated by the frame shown in the bottom image. The step height images and the corresponding cross sections which were calculated by the average height of (a) reduced and (b) oxidized states of the sample show the response of the redox-active PFS layer.

4. Conclusions

Here we propose a novel concept to quantitatively visualize sub nm height changes occurring in thin films of redox active polymers upon reversible electrochemical oxidation/reduction in-situ and in real-time combined electrochemistry imaging ellipsometry (EC-IE). Our approach is based on the use of micropatterned thin films, including patterns of inert (non-redox active) alkanethiols which function as zero level molecular reference. As the reference layer remains unperturbed upon electrode potential changes, it maintains a constant height during the experiment. Our method allows one to monitor the two step oxidation of surface grafted PFS on patterned areas of 600×400 μm^2 within two seconds. From imaging ellipsometry data a height change of 6 ± 1 Å can be deduced, which was also confirmed from electrochemical AFM measurements. The proposed method opens novel avenues to optically visualize minute and rapid changes occurring in redox active polymer films in a fast and non-invasive manner.

5. Acknowledgments

The work forms part of the research program of the Dutch Polymer Institute (DPI), projects DPI # 695. This project was also supported by NanoImpuls/NanoNed, the nanotechnology program of the Dutch Ministry of Economic Affairs and of the $MESA^+$ Institute for Nanotechnology of the University of Twente. Helpful discussions with Stefan Kooij are gratefully acknowledged. Excellent technical support from Clemens Padberg is gratefully acknowledged. Artwork was provided from NOLUX Media.

6. References

1 Halthur, T. J.; Claesson, P. M.; Elofsson, U. M. *J Am Chem Soc* **2004**, *126*, 17009-17015.
2 Harris, J. J.; Bruening, M. L. *Langmuir* **2000**, *16*, 2006-2013.
3 Campoy-Quiles, M.; Ferenczi, T.; Agostinelli, T.; Etchegoin, P. G.; Kim, Y.; Anthopoulos, T. D.; Stavrinou, P. N.; Bradley, D. D. C.; Nelson, J. *Nat Mater* **2008**, *7*, 158-164.
4 Papanu, J. S.; Hess, D. W.; Bell, A. T.; Soane, D. S. *J Electrochem Soc* **1989**, *136* 1195-1200.
5 Santonicola, M. G.; de Groot, G. W.; Memesa, M.; Meszynska, A.; Vancso, G. J. *Langmuir* **2010**, *26*, 17513-17519.
6 Sui, X. F.; Zapotoczny, S.; Benetti, E. M.; Memesa, M.; Hempenius, M. A.; Vancso, G. J. *Polym Chem-Uk* **2011**, *2*, 879-884.
7 Minko, S.; Sidorenko, A.; Stamm, M.; Gafijchuk, G.; Senkovsky, V.; Voronov, S. *Macromolecules* **1999**, *32*, 4532-4538.
8 Halthur, T. J.; Elofsson, U. M. *Langmuir* **2004**, *20*, 1739-1745.
9 Pasche, S.; De Paul, S. M.; Vörös, J.; Spencer, N. D.; Textor, M. *Langmuir* **2003**, *19*, 9216-9225.
10 Peter, M.; Hempenius, M. A.; Kooij, E. S.; Jenkins, T. A.; Roser, S. J.; Knoll, W.; Vancso, G. J. *Langmuir* **2004**, *20*, 891-897.
11 Carlin, C. M.; Kepley, L. J.; Bard, A. J. *J Electrochem Soc* **1985**, *132*, 353-359.
12 Asinovski, L.; Beaglehole, D.; Clarkson, M. T. *Phys Status Solidi A* **2008**, *205*, 764-771.
13 Jin, G.; Jansson, R.; Arwin, H. *Rev Sci Instrum* **1996**, *67*, 2930-2936.
14 Munteanu, S.; Garraud, N.; Roger, J. P.; Amiot, F.; Shi, J.; Chen, Y.; Combellas, C.; Kanoufi, F. *Anal Chem* **2013**, *85*, 1965-1971.
15 Svoboda, V.; Cooney, M. J.; Rippolz, C.; Liaw, B. Y. *J Electrochem Soc* **2007**, *154*, D113-D116.
16 Schmaljohann, D.; Nitschke, M.; Schulze, R.; Eing, A.; Werner, C.; Eichhorn, Y. J. *Langmuir* **2005**, *21*, 2317-2322.
17 Faiss, S.; Schuy, S.; Weiskopf, D.; Steinem, C.; Janshoff, A. *J Phys Chem B* **2007**, *111*, 13979-13986.
18 Körstgens, V.; Wiedersich, J.; Meier, R.; Perlich, J.; Roth, S. V.; Gehrke, R.; Müller-Buschbaum, P. *Anal Bioanal Chem* **2010**, *396*, 139-149.
19 Yu, Y.; Jin, G. *J Colloid Interf Sci* **2005**, *283*, 477-481.
20 Liu, L.; Chen, Y. Y.; Meng, Y. H.; Chen, S.; Jin, G. *Thin Solid Films* **2011**, *519*, 2758-2762.
21 Nguyen, P.; Gomez-Elipe, P.; I, M. *Chem Rev* **1999**, *99*, 1515-1548.
22 Whittell, G. R.; Manners, I. *Adv Mater* **2007**, *19*, 3439-3468.
23 Trippe, G.; Ocafrain, M.; Besbes, M.; Monroche, V.; Lyskawa, J.; Le Derf, F.; Salle, M.; Becher, J.; Colonna, B.; Echegoyen, L. *New J Chem* **2002**, *26*, 1320-1323.
24 Eloi, J. C.; Chabanne, L.; Whittell, G. R.; Manners, I. *Mater Today* **2008**, *11*, 28-36.
25 Kulbaba, K.; Manners, I. *Macromol Rapid Comm* **2001**, *22*, 711-724.
26 Ahmed, R.; Hsiao, M. S.; Matsuura, Y.; Houbenov, N.; Faul, C. F. J.; Manners, I. *Soft Matter* **2011**, *7*, 10462-10471.

27 Peter, M.; Lammertink, R. G. H.; Hempenius, M. A.; Vancso, G. J. *Langmuir* **2005**, *21*, 5115-5123.
28 Manners, I. *Chem Commun* **1999**, 857-865.
29 Peter, M.; Lammertink, R. G. H.; Hempenius, M. A.; van Os, M.; Beulen, M. W. J.; Reinhoudt, D. N.; Knoll, W.; Vancso, G. J. *Chem Commun* **1999**, 359-360.
30 Puzzo, D. P.; Arsenault, A. C.; Manners, I.; Ozin, G. A. *Angew Chem Int Edit* **2009**, *48*, 943-947.
31 Feng, X. L.; Cumurcu, A.; Sui, X. F.; Song, J.; Hernpenius, M. A.; Vancso, G. J. *Langmuir* **2013**, *29*, 7257-7265.
32 Sui, X. F.; Feng, X. L.; Song, J.; Hempenius, M. A.; Vancso, G. J. *J Mater Chem* **2012**, *22*, 11261-11267.
33 Lammertink, R. G. H.; Hempenius, M. A.; van den Enk, J. E.; Chan, V. Z. H.; Thomas, E. L.; Vancso, G. J. *Adv Mater* **2000**, *12*, 98-103.
34 Cheng, J. Y.; Ross, C. A.; Chan, V. Z. H.; Thomas, E. L.; Lammertink, R. G. H.; Vancso, G. J. *Adv Mater* **2001**, *13*, 1174-1178.
35 Clendenning, S. B.; Aouba, S.; Rayat, M. S.; Grozea, D.; Sorge, J. B.; Brodersen, P. M.; Sodhi, R. N. S.; Lu, Z. H.; Yip, C. M.; Freeman, M. R.; Ruda, H. E.; Manners, I. *Adv Mater* **2004**, *16*, 215-+.
36 Ramanathan, M.; Nettleton, E.; Darling, S. B. *Thin Solid Films* **2009**, *517*, 4474-4478.
37 Suarez, M. F.; Compton, R. G. *J Electroanal Chem* **1999**, *462*, 211-221.
38 Smela, E.; Gadegaard, N. *Adv Mater* **1999**, *11*, 953-+.
39 Schmidt, D. J.; Cebeci, F. C.; Kalcioglu, Z. I.; Wyman, S. G.; Ortiz, C.; Van Vliet, K. J.; Hammond, P. T. *Acs Nano* **2009**, *3*, 2207-2216.
40 Lizarraga, L.; Andrade, E. M.; Molina, F. V. *J Electroanal Chem* **2004**, *561*, 127-135.
41 Song, J.; Janczewski, D.; Guo, Y. Y.; Xu, J. W.; Vancso, G. J. *Nanoscale* **2013**, *5*, 11692-11698.
42 Song, J.; Janczewski, D.; Ma, Y. J.; van Ingen, L.; Sim, C. E.; Goh, Q. L.; Xu, J. W.; Vancso, G. J. *Eur Polym J* **2013**, *49*, 2477-2484.
43 Wilbur, J. L.; Kumar, A.; Kim, E.; Whitesides, G. M. *Adv Mater* **1994**, *6*, 600-604.
44 Xia, Y. N.; Kim, E.; Zhao, X. M.; Rogers, J. A.; Prentiss, M.; Whitesides, G. M. *Science* **1996**, *273*, 347-349.
45 Korczagin, I.; Lammertink, R. G. H.; Hempenius, M. A.; Golze, S.; Vancso, G. J. *Advances in Polymer Science* **2006**, *200*, 91-117.
46 Voskuhl, J.; Brinkmann, J.; Jonkheijm, P. *Curr Opin Chem Biol* **2014**, *18*, 1-7.
47 Acikgoz, C.; Hempenius, M. A.; Huskens, J.; Vancso, G. J. *Eur Polym J* **2011**, *47*, 2033-2052.
48 Xia, Y. N.; Whitesides, G. M. *Langmuir* **1997**, *13*, 2059-2067.
49 Kumar, A.; Biebuyck, H. A.; Whitesides, G. M. *Langmuir* **1994**, *10*, 1498-1511.
50 Tien, J.; Xia, Y.; Whitesides, G. M. *Thin Films* **1998**, *24*, 227-250.
51 Advincula, R.; Aust, E.; Meyer, W.; Knoll, W. *Langmuir* **1996**, *12*, 3536-3540.
52 Brandt, P. F.; Rauchfuss, T. B. *J Am Chem Soc* **1992**, *114*, 1926-1927.
53 Rulkens, R.; Lough, A. J.; Manners, I.; Lovelace, S. R.; Grant, C.; Geiger, W. E. *J Am Chem Soc* **1996**, *118*, 12683-12695.
54 Shi, W. Q.; Giannotti, M. I.; Zhang, X.; Hempenius, M. A.; Scönherr, H.; Vancso, G. J. *Angew Chem Int Edit* **2007**, *46*, 8400-8404.
55 Chao, T. S.; Lee, C. L.; Lei, T. F. *J Electrochem Soc* **1991**, *138*, 1756-1761.